Appl. Phys. B 62, 21–27 (1996)

Applied Physics B Lasers and Optics

Linewise Raman-Stokes/anti-Stokes temperature measurements in flames using an unintensified charge-coupled device

J. A. Wehrmeyer, S. Yeralan, K. S. Tecu

Mechanical and Aerospace Engineering Department, University of Missouri-Columbia, Columbia, MO 65211, USA
(Fax: +1-314/884-5090, E-mail: WEHRMEYER@ecvax2.ecn.missouri.edu)

Received: 6 June 1995/Accepted: 28 August 1995

Abstract. One-dimensional, spatially resolved (linewise), temporally averaged Stokes/anti-Stokes temperature measurements with 200 μm spatial resolution and 6% precision uncertainty are demonstrated in an opposed-jet-diffusion flame of air vs N_2-diluted H_2 using the Raman-Stokes/anti-Stokes technique. The Stokes/anti-Stokes temperature profile is compared to temperature measurements obtained using all major species' Q-branches and differences between the two sets of results are discussed. In addition, single-pulse, linewise measurements with 710 μm spatial resolution and 19% precision uncertainty are also demonstrated. To the authors' knowledge this is the first report of linewise Stokes/anti-Stokes temperature measurements in flames. Simultaneous measurements of the N_2 Stokes and anti-Stokes vibrational Q-branches are obtained by using an unintensified Charge-Coupled Device (CCD) that is gated by a ferro-electric liquid crystal light valve and/or a low duty cycle optical chopper to suppress detected flame luminosity. This detection system provides increased detection efficiency, dynamic range, and imaged spectral range over an intensified CCD, allowing spatially resolved Stokes and anti-Stokes signals to be imaged onto one detector.

PACS: 07.65; 78.30; 82.20

Multipoint, non-intrusive temperature and gas species concentration measurements are important tools to study combustion scalars. One laser-based technique, spontaneous Raman scattering, has been used to obtain one-dimensional, spatially resolved (linewise) temperature and gas species concentration measurements in flames [1–3]. Linewise, rather than pointwise measurements, are desirable because they provide not just information about a scalar but also information about that scalar's gradient. These past works have generally reduced the Raman signals to temperature measurements by a priori knowledge of the flowfield pressure, since the Raman data, which are directly proportional to gas species number density, can then be related to temperature by using the perfect gas equation-of-state. One type of pressure-independent Raman temperature measurement technique exploits the temperature dependence of the ratio of a gas specie's Stokes and anti-Stokes vibrational Q-branches [4]. The Stokes/anti-Stokes ratio is density (hence pressure) insensitive and thus can provide a vibrational-temperature measurement in pressure-varying flows. The straightforward, theoretical relationship between the Stokes/anti-Stokes ratio and temperature also provides for explicit, one-step data reduction, in contrast to the iterative data reduction procedures used in previous linewise Raman efforts [1, 2]. However, the Stokes/anti-Stokes technique can be used only to examine gas flows with significant amounts of vibrationally excited molecules and thus cannot be used in low-temperature situations.

The Stokes/anti-Stokes technique has been used extensively in the past for pointwise temperature measurements in constant pressure [5–7] and variable pressure (supersonic) H_2–air flames [8] but has not been demonstrated as a viable technique for linewise temperature measurements. With the development of high efficiency, spatially sensitive photodetectors, and the advent of high-efficiency holographic notch filters, it is now possible to obtain anti-Stokes signals of sufficient intensity to allow spatially resolved linewise measurements. This paper describes linewise temperature measurements in a laminar H_2–N_2–air flame using the Stokes/anti-Stokes technique. Multipulse averaging is used in the steady flame to improve measurement uncertainties. Single-pulse, linewise temperature measurements in a fluctuating flowfield are also reported. To these authors' knowledge, this is the first report of linewise Stokes/anti-Stokes temperature measurements in flames.

A Charge-Coupled Device (CCD) is used as the detection device for the spectrally and spatially resolved Raman measurements. Specifically, an unintensified CCD is employed because of the enhanced signal strength and the increased imaging area that it provides over intensified CCDs that have been used for past work [1–3]. It is these increases in detection efficiency, dynamic range, and imaged spectral range provided by the unintensified CCD

that allow successful linewise Stokes/anti-Stokes temperature measurements to be made.

1 Experimental system

A system schematic is shown in Fig. 1. The 532 nm, 300 mJ, vertically polarized, pulsed output of a 10 Hz frequency-doubled Nd:YAG laser is the excitation source. The laser output is focused by either a 0.75 or 1.5 m focal length lens down the cylindrical axis of an opposed jet burner. In this manner, linewise temperature measurements are obtained in laminar diffusion flames through the flames' axis of symmetry. The beam waist provided by this arrangement is between 0.5 and 0.75 mm. Spontaneous Raman scattering produced in the diffusion flame is imaged onto the entrance slit of a 0.25 m spectrograph, with the slit's long dimension situated parallel to the laser beam. A holographic notch filter suppresses laser-line scattering from entering the spectrograph. This filter has an optical density greater than 4.0 at 532 nm and an 80% transmittance outside of a 10 nm bandwidth notch.

The Raman signals are imaged onto a cryogenically-cooled, unintensified CCD that is "gated" for a 40 μs exposure by a Displaytech Ferro-electric Liquid-Crystal light valve (FLC). Gating at this exposure time sufficiently discriminates the pulsed Raman signals from the constant flame luminosity produced in the H_2–air flames examined. A 10 Hz low-duty-cycle optical chopper (~1 ms open state) is also used to block the FLC's off-state light transmission (0.03%). Even though the FLC has an open-state transmission efficiency of only 40%, this detection system provides increased detection efficiency over one with an intensified CCD because of the unintensified CCD's higher quantum efficiency (~0.40) compared to an intensifier photocathode's (~0.07). An experimental comparison between this unintensified CCD/FLC system and a fiber-optically coupled intensified CCD has demonstrated that the unintensified system provides a 40% improvement in the signal/noise ratio over the intensified version, at least for the low luminosity H_2–N_2–air flames examined [10].

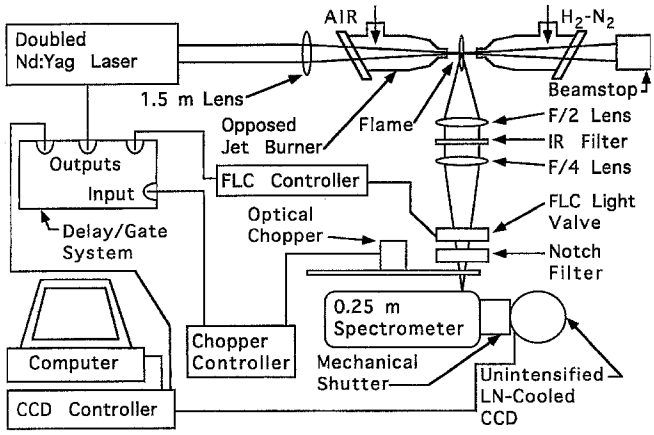

Fig. 1. Schematic of unintensified CCD Raman system

Additionally, the unintensified configuration allows a larger spectral range to be imaged, since a typical intensifier photocathode limits a rectangular image to a 25 mm diagonal length. The 27.6 mm × 6.9 mm CCD used in this work (EEV 1024 × 256 pixels front-side illuminated) images 138 nm of spectral range and 2.56 mm of laser beam axial length. The sample volume length of the laser beam is determined by the magnifications of the light collection system and spectrograph: 2.0 and 1.35, respectively. The 473 nm N_2 anti-Stokes and 607 nm N_2 Stokes vibrational Q-branch signals are both simultaneously imaged onto the CCD, though just within the CCD's wavelength limits.

The CCD is binned into superpixels to allow 32 separate locations to be measured down the axis of the laser beam, with each location corresponding to 1/32 of the 2.56 mm imaging extent, or 80 μm. The effective spatial resolution of each location is also affected by the laser beam waist and by the imperfect focusing of the light-collection system. When using the 1.5 m laser focusing lens and the above-mentioned binning, overall spatial resolution has been experimentally determined to be ~200 μm by imaging the graybody emission coming from 15 μm diameter silicon carbide fibers [11].

Dark noise on the CCD is virtually eliminated by its cryogenic cooling and readout noise is reduced to less than one A/D count by reading the CCD at 25 MHz. A 14 bit CCD controller is used, and there is a constant voltage bias equivalent to about 30 counts. Thus the useful dynamic range of this unintensified CCD ranges well over three orders of magnitude.

Using an experimental detection system based upon an unintensified CCD allows several important criteria to be met if linewise Stokes/anti-Stokes temperature measurements are to be made. The system has to have the highest detection efficiency possible and has to be able to simultaneously measure both the Stokes and anti-Stokes signals of at least one gas specie. This system has already been demonstrated to be more sensitive than visible Raman systems using intensified CCD's. While Raman systems using ultraviolet lasers have higher sensitivities due to the increase in Raman cross section, they do not currently have high-efficiency holographic notch filters available for simultaneous Stokes/anti-Stokes imaging onto one CCD. The dynamic range of the unintensified CCD is larger by at least an order of magnitude over an intensified CCD, which allows simultaneous imaging of the relatively weak anti-Stokes signal and the relatively strong Stokes signal onto one CCD. The increased dynamic range afforded by an unintensified CCD has been exploited for coherent anti-Stokes Raman spectroscopy but has not previously been used for Stokes/anti-Stokes spontaneous Raman work [12]. Another criterion met by this system configuration is to provide the needed spectral range while at the same time maintaining adequate spectral resolution, which is limited by the source image width. Increasing the reciprocal linear dispersion of the spectrograph, in order to provide the same spectral range for a smaller area intensified CCD, would result in overlap of the various Raman signals and greatly complicate data reduction.

2 Multipoint, time-averaged Stokes/anti-Stokes temperature measurements

To demonstrate linewise Stokes/anti-Stokes temperature measurements and their utility, the experimental system is used to investigate an opposed jet laminar diffusion flame. This flame is created by impinging a jet of air onto a jet of H_2 diluted by N_2 (50% mole fraction). The jets are formed by 4 to 1 contraction-ratio nozzles with 5 mm exit dias. The small diameters are used to allow higher exit velocities to be achieved while maintaining laminar flow. The separation distance between the jet exits is 7.5 mm. The laser beam travels horizontally down the axis of symmetry of this cylindrical configuration. To reduce relative shot noise, Raman signals from 200 single-pulse measurements of this laminar flame are averaged directly on the CCD.

Figure 2 shows spatially resolved Stokes/anti-Stokes spectra obtained from the opposed jet burner when the flow rates exiting the nozzles are 4.7 l/min air, 3.3 l/min H_2, and 3.3 l/min N_2. Axial position locations are referenced to the air-nozzle location. Of all the anti-Stokes signals present in Fig. 2, only the N_2 vibrational Q-branch is appreciably apparent. To better view the anti-Stokes signals, Fig. 3 uses an expanded vertical scale and displays only the anti-Stokes wavelengths. In addition to the N_2 vibrational Q-branch, the O_2 vibrational Q-branch and an H_2 rotational O-branch can be discerned. These latter two signals do not occur throughout the entire flame, are less intense than the N_2 signal, and so are not used to derive temperature, although they could be used to corroborate N_2 vibrational temperatures in limited regions of the flame. A scale comparison between Figs. 2 and 3 shows over an order-of-magnitude difference in typical signal strength between the Stokes and anti-Stokes signals, pointing out the need for large dynamic range.

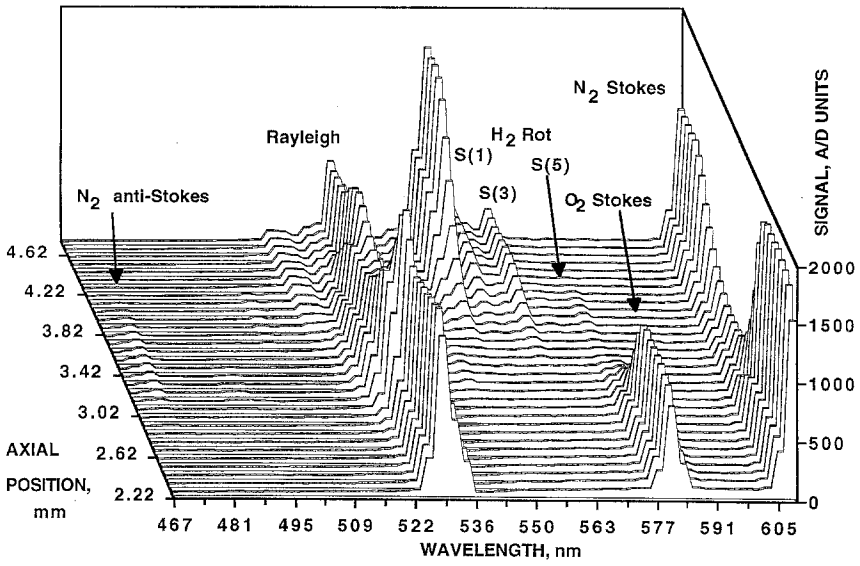

Fig. 2. Spatially resolved Stokes/anti-Stokes Raman spectra obtained down axis of a laminar opposed jet H_2–N_2 vs air diffusion flame. 200 shot integration

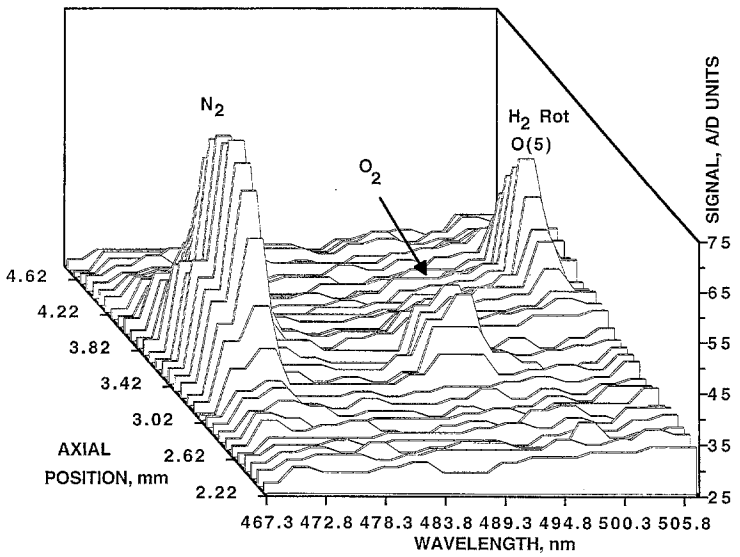

Fig. 3. Close-up view of anti-Stokes Raman spectra from Fig. 2

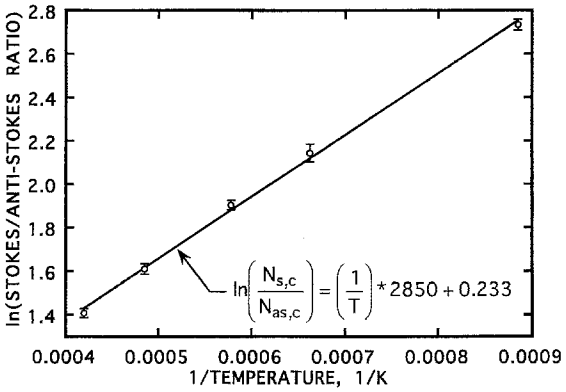

Fig. 4. Average of the natural log of the Stokes/anti-Stokes ratio vs inverse of thermocouple-measured temperature for N_2 vibrational Raman Q-branches in five H_2–air flames of different stoichiometry produced above a Hencken burner

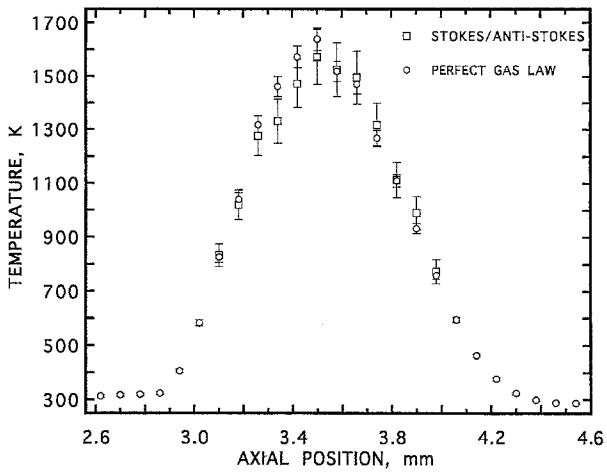

Fig. 5. Temperature profiles derived from Stokes/anti-Stokes ratio and perfect gas law for the opposed jet diffusion flame of Fig. 2

To transform the Raman data of Figs. 2 and 3 into temperature measurements, the total Q-branch signals must first be determined. This is accomplished by adding the signals from the superpixels that represent the wavelength range for the Stokes and anti-Stokes Q-branches. This sum will contain, in addition to the Raman signal, a contribution from the constant voltage bias of the A/D card and interference from fluorescence, stray light, and flame emission. All of these are corrected for by sampling superpixels spectrally proximate to the Raman wavelengths and using these as correction channels. This can be done because the interferences are relatively broadband and are not greatly affected by small changes in wavelength. The interference-corrected Stokes signal, $N_{s,c}$, is then the difference between the uncorrected Stokes signal, $N_{s,u}$ and its interference correction channel $N_{s,int}$. Likewise, the interference-corrected anti-Stokes signal, $N_{as,c}$, is $N_{as,u} - N_{as,int}$. For a stoichiometric H_2–air flame $N_{as,c} \approx 80$ counts, compared to $N_{as,int} \approx 35$ counts. At the flame temperatures examined in this paper there is a slight problem with an H_2 anti-Stokes rotational Raman line, the O(9) at 485 nm, contaminating $N_{as,int}$. Thus this correction channel is itself corrected for rich flames by relating the O(9) signal of H_2 to its strong S(3) at 563 nm. The relationship between the two H_2 lines is temperature-dependent, with this effect modeled by the ratio of their Boltzmann fractions: $\exp[-4295\ \mathrm{cm}^{-1}\ (1.4388\ \mathrm{cm\ K})/T]$, where $4295\ \mathrm{cm}^{-1}$ is the difference between the rotational energy term values for the ninth and third H_2 rotational levels, $5001\ \mathrm{cm}^{-1}$ and $706\ \mathrm{cm}^{-1}$, respectively.

To relate the spectrally integrated Stokes and anti-Stokes signals to temperature, T, an experimental system calibration is performed. The two opposed jet nozzles are both moved axially away from the sample volume by ~ 10 mm each. This allows a 25.4 mm diameter Hencken multielement flat flame diffusion burner to be positioned near the sample volume. By sampling the post-flame gases from this burner, a calibration can be obtained since temperatures are also measured in this constant flowfield by radiation-corrected, uncoated, 50 μm diameter Pt30% Rh vs Pt6%Rh thermocouples. Treating each of the measurement locations as an independent measurement of the constant flowfield, averages of $\ln(N_{s,c}/N_{as,c})$ for N_2 are obtained at five different calibration conditions. Figure 4 shows these data (with error bars indicating two sample standard deviations of the 32 measurements) as functions of inverse temperature. A best-fit straight line passes through the ranges for all five averages and has a slope of 2849 K, which is about 85% of the expected slope of 3354 K (the characteristic vibrational temperature of N_2). This can be explained by the fact that not all of the Stokes vibrational Q-branch is measured, because of the imaging limits of the CCD and spectrograph. The spectrograph is tuned to completely image the weak anti-Stokes signal. However, this tuning cuts off a portion (15%) of the Stokes signal on its long wavelength side. With increasing temperature there is relatively more signal in the short wavelength portion of the Stokes vibrational Q-branch, which acts to slightly decrease the sensitivity of the Stokes/anti-Stokes measurement to temperature.

After obtaining calibration information, the data of Figs. 2 and 3 are transformed into temperature measurements, which are displayed in Fig. 5. Also with the Stokes/anti-Stokes temperature measurements are displayed temperature measurements using the perfect gas law. These measurements were obtained from the Stokes vibrational Q-branches of all major species, data which is not shown in this paper but is described elsewhere [10, 11]. Precision uncertainties (95% confidence level) are shown for both sets of data, with the Stokes/anti-Stokes precision uncertainties obtained using the error analysis described in the following section. The Stokes/anti-Stokes temperature measurement uncertainties generally are $\sim 6\%$. The perfect gas law temperature measurements have better precision uncertainties because relatively strong Stokes signals from the four major species of this H_2–air flame are used. In general, the agreement between the two methods is good, except on the air side of the flame near the peak temperature location. Here the Stokes/anti-Stokes temperature measurements are consistently lower than the perfect gas law temperature

measurements. This can at least be partially explained by the fact that the perfect gas law method uses the Stokes signals from only the four major species (O_2, N_2, H_2O, and H_2) and disregards the contribution to total density provided by the minor species. Flame modeling for a similar flow field has shown that minor species, especially H, O, and OH, provide up to an additional 3% to the total number density near the peak temperature location [13]. This suggests that there should be ~50 K discrepancy between the two methods at this location, with the perfect gas law overpredicting the temperature.

3 Multipoint, single-pulse Stokes/anti-Stokes temperature measurements

A major application of the Stokes/anti-Stokes technique is for pressure-varying flows where the unknown pressure prevents using the perfect gas law to relate measured density to temperature. However, such flows are usually turbulent and hence the Stokes/anti-Stokes method must be applied on a single-pulse basis. In order to compensate for the reduced signal of a single-pulse measurement compared to time-averaged data, a larger spatial resolution must be used.

The precision uncertainty in a single-pulse Stokes/anti-Stokes temperature measurement, u_T, is approximated by [14]:

$$u_T = \sqrt{\left(\frac{\partial T}{\partial N_{s,u}} u_{Ns,u}\right)^2 + \left(\frac{\partial T}{\partial N_{as,u}} u_{Nas,u}\right)^2 + \left(\frac{\partial T}{\partial N_{s,int}} u_{Ns,int}\right)^2 + \left(\frac{\partial T}{\partial N_{as,int}} u_{Nas,int}\right)^2}, \quad (1)$$

where each precision uncertainty $u_{Ni,j}$ is for signal $N_{i,j}$ expressed in number of photoelectrons. The partial derivatives in (1) are obtained from the theoretical relationship between T and $\ln(N_{s,c}/N_{as,c})$ [4]. Each $u_{Ni,j}$ is assumed to have the following form:

$$u_{Ni,j} = \sqrt{N_{i,j} \times 7 \text{ photoelectrons/count} + (\text{rms readout noise})^2}. \quad (2)$$

Equation (2) gives the shot noise as the square root of the product of the signal, in counts, times the number of photoelectrons per count, which is estimated to be 7 for the A/D circuitry of this work. The rms readout noise is estimated to be 0.8 counts, or 6 photoelectrons. The above equations show that for precise temperature measurements it is necessary to maximize the signal strength of $N_{s,u}$ and $N_{as,u}$ with respect to $N_{s,int}$ and $N_{as,int}$ and with respect to readout noise. This is accomplished in the previous section by time-averaging and by using the FLC with the optical chopper to suppress detected flame luminosity. However, because of the low signal levels of single-pulse measurements it is more advantageous to remove the FLC to increase the Raman signal strength at the expense of relatively higher interference. In this way, the effect of readout noise is reduced.

To arrive at an experimental determination of single-pulse precision uncertainty, Stokes/anti-Stokes temperature measurements are obtained in the steady flowfield of the Hencken burner supporting a lean H_2–air flame ($T = 1730$ K, equivalence ratio = 0.5). One hundred measurements are obtained for each of the following binning arrangements for the 256 pixel width of the CCD: 256 pixels, corresponding to a sample volume length of 2.56 mm; 128 pixels, for two linewise measurements with 1.28 mm sample-volume lengths; 64 pixels, four at 0.64 mm; and 32 pixels, eight at 0.32 mm. The effective spatial resolution in these measurements is the sample-volume length plus an additional 70 μm from imperfect focusing and a finite-sized laser beam waist. Table 1 lists the relative standard deviations for the four measurement samples, along with relative precision uncertainties calculated using (1) and (2). Generally, good agreement is seen between the uncertainties and standard deviations.

To demonstrate single pulse, linewise Stokes/anti-Stokes temperature measurements in a fluctuating flowfield, the Hencken burner is moved transversely so that the shear layer between the post-flame zone and the slower moving N_2 co-flow is sampled. The CCD is binned to provide four linewise measurements with 0.64 mm spatial resolution. In the wavelength direction, the CCD is binned to completely measure $N_{as,u}$ within one superpixel to avoid the compounding of readout and digitization errors. This is also done for $N_{as,int}$, $N_{s,int}$, and $N_{s,u}$, with the rest of the wavelength direction remaining unbinned. The resulting four Raman spectra are displayed in Fig. 6.

By using a data reduction procedure that relies upon an experimental calibration as shown in Fig. 4, the data of Fig. 6 are reduced to the four linewise temperature measurements of Fig. 7. Error bars indicate the range of precision uncertainty (typically 19%) estimated using (1) and (2). A temperature difference of over 500 K can be seen to occur in a distance of about 2.5 mm, indicating the need for good spatial resolution in temperature measurements at this location.

Table 1. Precision errors for single-pulse Stokes/anti-Stokes temperature measurements in a lean (1730 K, 0.5 equivalence ratio) H_2–air flame

No. of measurements along line	Sample volume length [mm]	Exp. rel. std. dev. 100 shot sample [%]	Calculated rel. precision uncertainty [%]
1	2.56	7.6	7.9
2	1.28	11.2	12.4
4	0.64	17.7	19.5
8	0.32	30.9	30.5

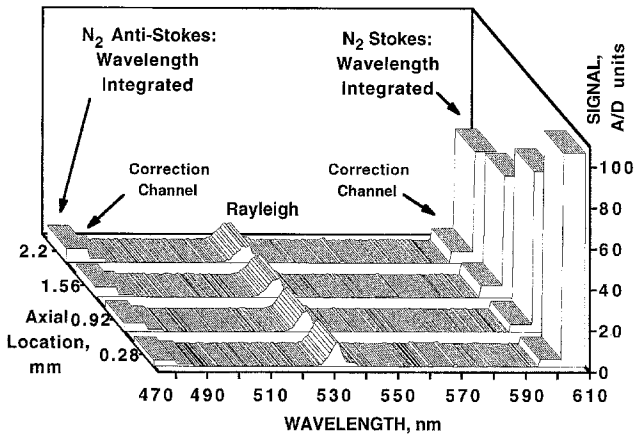

Fig. 6. Single-pulse Stokes/anti-Stokes Raman spectra obtained in shear layer between lean H_2–air flame and slower N_2 co-flow

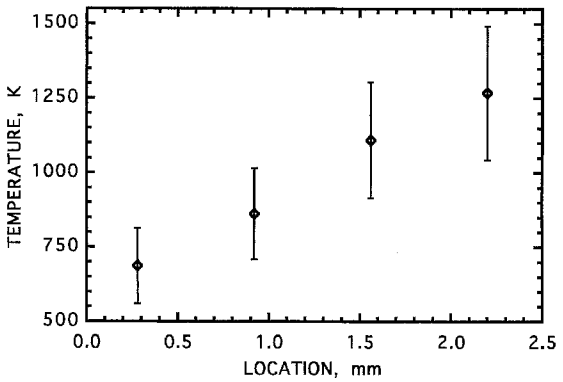

Fig. 7. Stokes/anti-Stokes temperature measurements in shear layer between lean H_2–air flame and slower N_2 co-flow

4 Summary

In summary, one-dimensional, temporally averaged, spatially resolved Raman Stokes/anti-Stokes temperature measurements have been demonstrated in a laminar H_2–N_2–air diffusion flame. Single-pulse, linewise temperature measurements have also been demonstrated. This technique obtains the N_2 vibrational temperature by using an unintensified CCD camera that simultaneously images both the Stokes and anti-Stokes N_2 vibrational Q-branch Rama signals. An unintensified CCD is used because of its increased quantum efficiency over intensified CCDs. The increased image size of the unintensified CCD over intensified versions also allows the needed spectral range and spectral resolution to be simultaneously achieved. Adequate suppression of the detected flame luminosity is accomplished, at least for low-luminosity H_2-fueled flames, by gating the CCD to 40 μs with an FLC light valve and/or by using a low-duty-cycle optical chopper. The resulting higher detection efficiency of this system, and its increased dynamic range over an intensified CCD, allow spatially resolved anti-Stokes signals to be obtained simultaneously with their stronger Stokes counterparts, even when there is a variation by over an order of magnitude in their relative signal strengths.

Multipoint Stokes/anti-Stokes temperature measurements with 200 μm spatial resolution and 6% uncertainty are demonstrated in a laminar H_2–N_2 vs air diffusion flame by multipulse averaging of 200 laser shots. Agreement is good between the Stokes/anti-Stokes temperature profile and one obtained using the perfect gas law coupled with all four major-species Stokes signals. However, there is disagreement between the profiles near the peak-temperature location on the diffusion flame's air side. Any discrepancy between the two methods is expected to be greatest at this location because the perfect gas law method disregards the contributions to total density made by minor species.

The single-pulse temperature profile of Fig. 7, obtained in the shear layer between a lean H_2–air flame and its slower N_2 co-flow, reveals significant temperature gradients over the 2.56 mm measurement region, pointing out the need for spatially resolved linewise Raman measurements. For the four temperature measurements of Fig. 7, a 0.64 mm sample volume length is used, allowing a 19% precision uncertainty in the temperature measurements. Further application of this technique to linewise temperature measurements in compressible, reacting flows is straightforward, though vibrational non-equilibrium must be considered [8].

To improve the measurement precision in either the time-averaged or single-pulse measurements, signal strength must be enhanced. Signal strength enhancements include: use of a higher power and/or shorter wavelength laser (although the FLC light valve's lower operational wavelength is 400 nm), replacement of the sheet polarizers of the FLC with high-efficiency crystal polarizers, optimization of the thickness of the FLC quarter-wave plate for the wavelength region of interest, larger collection system etendue, and backside-illuminated CCDs with their higher quantum efficiency (especially at the anti-Stokes wavelength) than the front-side illuminated CCD used in this work.

Acknowledgements. The authors are grateful to the National Science Foundation (grant CTS-9210988) and the Engineering Foundation (grant RI-A-91-06) for supporting this work.

References

1. S.P. Nandula, T.M. Brown, R.W. Pitz, P.A. DeBarber: Opt. Lett. **19**, 414 (1994)
2. J.H. Frank, K.M. Lyons, D.F. Marran, M.B. Long, S.H. Stårner, R.W. Bilger: In *Proc. 25th Symp. (Int'l.) on Combustion* (The Combustion Institute, Pittsburgh, PA 1994) p. 1159
3. W. Reckers, L. Hüwel, G. Grünefeld, P. Andresen: Appl. Opt. **32**, 907 (1993)
4. M.C. Drake, M. Lapp, C.M. Penney: In *Temperature: Its Measurement and Control in Science and Industry*, ed. by J.F. Schooley (AIP, New York 1982) vol. 5, p. 631
5. M.C. Drake, R.W. Pitz, M. Lapp: AIAA J. **24**, 905 (1986)
6. P. Magre, R. Dibble: Combust. Flame **73**, 195 (1988)
7. T.S. Cheng, J.A. Wehrmeyer, R.W. Pitz: Combust. Flame **91**, 323 (1992)
8. T.S. Cheng, J.A. Wehrmeyer, R.W. Pitz, O. Jarrett, Jr., G.B. Northam: Combust. Flame **99**, 157 (1994)

9. G. Placzek: In *Handbuch der Radiologie*, Heft 6, Teil 2, ed. by E. Marx (Akademischer Verlag, Leipzig 1934)
10. J.A. Wehrmeyer, S. Yeralan, K.S. Tecu: Opt. Lett. **20**, 934 (1995)
11. J.A. Wehrmeyer, S. Yeralan, K. Tecu: AIAA Joint Propulsion Conf., San Diego, CA (July 1995) Paper 95-3114
12. I. Plath, W. Meier, W. Stricker: Op. Lett. **17**, 79 (1992)
13. G. Dixon-Lewis, M. Missaghi: In *Proc. 22nd Symp. (Int'l.) on Combustion* (The Combustion Institute, Pittsburgh, PA 1988) pp. 1461–1470
14. S.J. Kline, F.A. McClintock: Mech. Eng. **3**, 8 (1953)